Available online at www.CivileJournal.org

Civil Engineering Journal

(E-ISSN: 2476-3055; ISSN: 2676-6957)

Vol. 11, No. 08, August, 2025

Experimental and Numerical Modeling for the Impact of Freezing Temperatures Reduction on the Mechanical Properties of Frozen Sand

Wisam R. Hasan [1*], Hussein H. Karim [1], Saad F. Al-Wakel [1]

[1] *Civil Engineering Department, University of Technology- Iraq, Baghdad, Iraq.*

Received 13 March 2025; Revised 23 June 2025; Accepted 07 July 2025; Published 01 August 2025

Abstract

Artificial ground freezing (AGF) is an approach that uses heat extraction to congeal in situ soil to improve soil quality temporarily. This technology is ecologically sustainable and has minimal adverse effects on soil and groundwater. AGF is widely used in subterranean construction, providing temporary support and groundwater sealing. Nevertheless, precisely simulating the mechanical characteristics of frozen soils with dependable constitutive models presents significant challenges for scientists and engineers. Frozen soil, consisting of ice, liquid water, solid particles, and pore air, is a distinctive geological substance with heightened sensitivity to temperature and external influences. Experimental studies have shown that the mechanical properties of frozen soils are significantly influenced by temperature, confining pressure, strain rate, stress path, and stress level. Numerical simulation offers a superior approach for forecasting soil qualities, particularly in artificial frozen soil technologies for excavations like tunnels and mines. This research examines the impact of varying freezing temperatures and pressures on soil characteristics. This research employs experiments and numerical analysis using Mohr-Coulomb and hardening soil models. The experimental results indicated that the elastic modulus almost increases linearly by a rate of 90000 kN/m² with 1ºC drops below 0ºC. The unconfined compressive strength increased by 2068 kN/m² for each 1°C decrease from 0 to -2°C. Within the temperature range of -2°C to -10°C, the rate of increase is 529 kN/m². The apparent cohesion increased by 238.75 kN/m² for each 1°C decrease from 0 to -2°C. Within the temperature range of -2°C to -10°C, the rate of increase is 66.25 kN/m². A nonlinear association between temperature decrease and tensile stress rise was observed. Numerical analysis shows that as confined pressure increases and temperature decreases, materials can either get stronger or weaker; the Mohr-Coulomb and HS models show stress-strain curve behavior that matches what was found in experiments.

Keywords: AGF; Frozen Soil; Unfrozen Soil; Temperature; Constitutive Model.

1. Introduction

Artificial ground freezing (AGF) is a method that entails the temporary congelation of in situ soil by heat extraction to enhance soil quality. AGF offers several technical advantages, especially when other soil stabilizing methods are impractical. This technology is ecologically sustainable and does not have lasting adverse effects on soil and groundwater because of its reversible characteristics [1-3]. AGF methods are extensively used in subterranean construction, where artificially frozen soils provide temporary support and groundwater sealing by increasing soil modulus and reducing hydraulic conductivity. Using trustworthy constitutive models to accurately

* Corresponding author: bce.20.40@grad.uotechnology.edu.iq

http://dx.doi.org/10.28991/CEJ-2025-011-08-023

simulate the mechanical properties of frozen soils is crucial for scientists and engineers. Artificial ground freezing (AGF) techniques, such as shafts, tunnels, and deep excavations in difficult geological conditions, are used in mining and urban development, as well as engineering construction in permafrost regions, depends heavily on frozen soils [4, 5].

Over the past ten years, artificial ground freezing (AGF) has been used in subsurface engineering as a ground enhancement technique with amazing results. Artificial soil freezing methods have increased due to their advantages in promoting excavations, environmental sustainability, and improved safety relative to other procedures [6, 7].

The presence of ice significantly alters the mechanical performance of frozen soils, resulting in substantial differences in their mechanical behaviors compared to unfrozen soils [8-10]. Furthermore, the ice present in frozen soils significantly influences mechanical properties, enhancing the cohesive strength of soil solids and resulting in a nonzero tensile strength of the frozen soil [11]. Reports indicate that the cementation of ice and the intrinsic strength of the soil matrix contribute to the enhanced stability of frozen soils [12, 13].

Frozen soil is a distinct geological material composed of ice, unfrozen water, solid particles, and pore air. Analogous to the fundamental traits of unfrozen geomaterials, variations in ice content influence the mechanical properties of frozen soil. Frozen soil has heightened sensitivity to internal characteristics such as composition, content, size, and structure, in addition to being more vulnerable to external influences like temperature and applied force. Numerical simulation provides an advanced method for predicting soil properties and improving comprehension, especially in artificial frozen soil technologies for excavations such as tunnels and mines. The Finite Element Method (FEM) is a widely utilized computational technique for simulating soil behavior, especially in assessing the stress-strain properties of frozen soils [14-16].

The diverse configurations and heightened temperature sensitivity of frozen soils render their mechanical behaviors more intricate than those of unfrozen soils [17]. Temperature significantly affects the mechanical properties of frozen soils, as evidenced by numerous laboratory studies (e.g., French [18]). The ice content, influenced by temperature, affects soil's mechanical characteristics by displacing or adhering grains together. The impact of several parameters (such as temperature, confining pressure, strain rate, stress path, and stress level) on the mechanical characteristics of frozen soils has been thoroughly investigated in a number of experimental investigations carried out up to this point under static loadings. Additionally, it provides crucial information for the creation of constitutive models and engineering designs; these experiments are necessary for comprehending how frozen soils react to static loadings [19-21].

Yuanming et al. [22] demonstrated that, for constant confining pressure, a drop in temperature results in increased stiffness in the soil mixture. Zhu & Carbee [23] found a similar trend between the modulus of Young and temperature but found that artificially frozen soil has a lower Young's modulus than naturally frozen soil at equivalent temperatures, especially in silty soils. This discrepancy may be due to the higher strain levels used in the study, but the exact strain value is not explicitly stated.

This research aims to examine the impact of varying freezing temperatures and pressures on soil characteristics. This research employs experiments and numerical analysis using Mohr-Coulomb and hardening soil models.

2. Methodology

2.1. Project Overview

The earlier analysis of the proposed Baghdad metro in Baghdad City in 1980 offered two routes for each line, as shown in Figure 1, and the newest research by French company Systra has embraced the same concept. The tunnel is a circular cross-section with an outside diameter of 6.3 meters and a concrete lining thickness of 0.3 meters. The tunnel's vertical depth varies throughout its length, depending on the geological part of Baghdad City [24].

There are numerous terminologies for describing a tunnel's vertical depth. Figure 2 represents a standard vertical depth for two routes of the Baghdad metro.

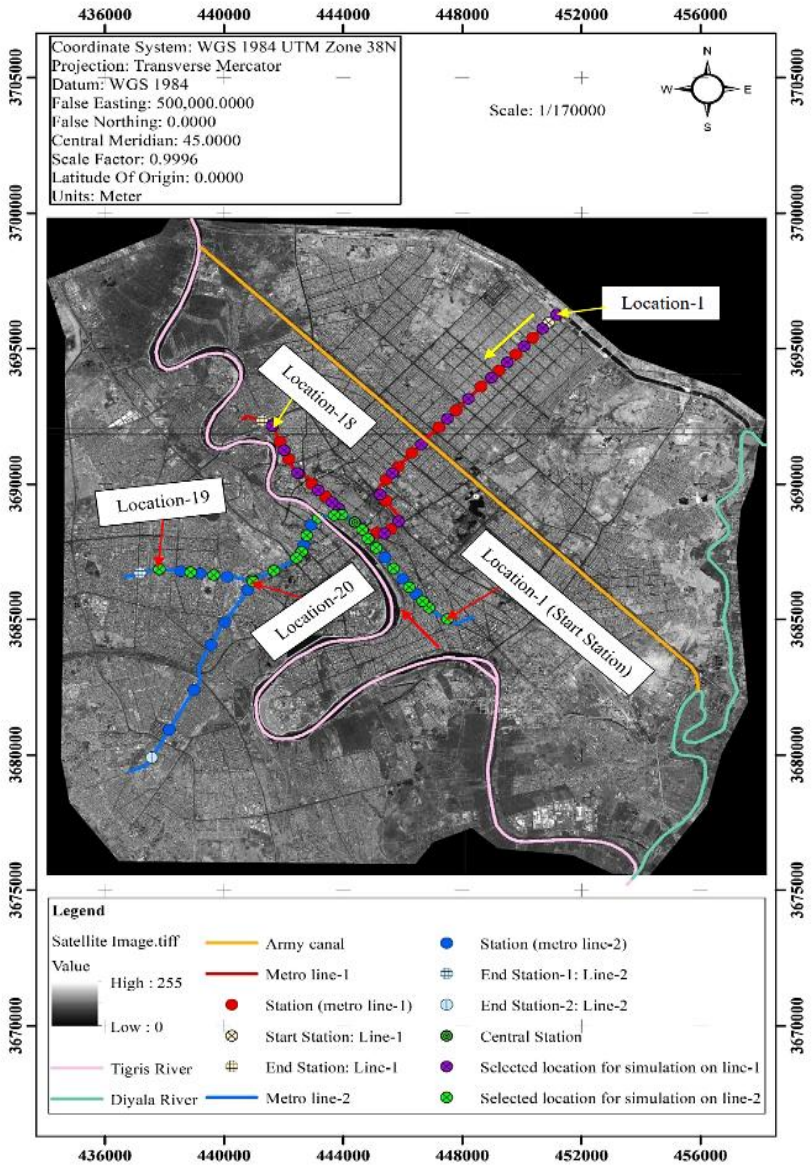

Figure 1. Plotting the Baghdad metro layout using a satellite [24]

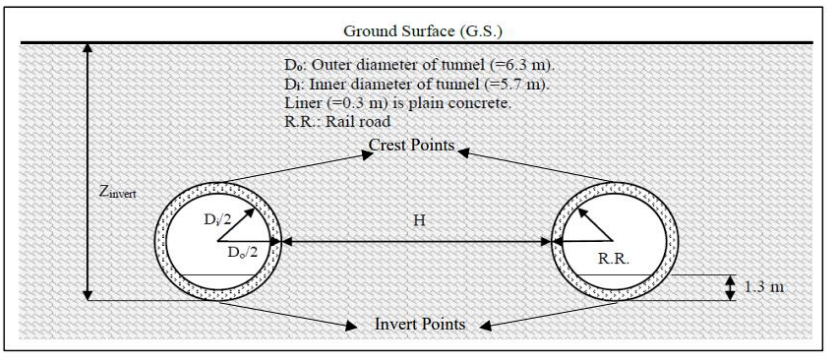

Figure 2. Typical vertical depth photograph of the city (with 60 cm resolution) [24]

2.2. Selection of Sample Materials

As mentioned above, the proposed metro routes for Baghdad are shown in Figure 1. Places were chosen for experiments, and a numerical simulation study of tunnel excavation work before, during, and after excavation. We collected samples from boreholes near site locations 19 and 20. The granular soil was identified as SP (poorly graded) upon initial examination of the unfrozen soil samples. Table 1, which displays the physical characteristics of the soil, was created using the particle size distribution curves, as seen in Figure 3.

Table 1. Physical characteristics of soil

Soil classification	SP
Saturated density, kN/m^3	18
The angle of friction, degree	35
Specific gravity, Gs	2.67
Gravel, %	5
Sand, %	93.5
Clay and silt, %	1.5
Coefficient of uniformity, Cu	2.5
Coefficient of curvature, Cc	1.31
Cohesion, c	0

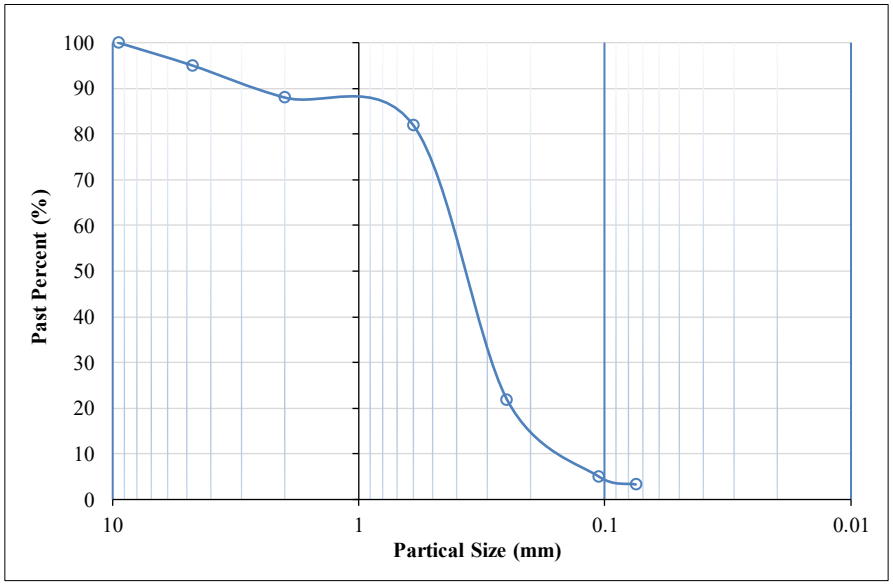

Figure 3. Particle Size Distribution Curves

2.3. Sample Preparation

For the triaxial testing, we created cylindrical specimens that were 200 mm in height and 100 mm in diameter. All the soil samples were reshaped to keep the same void ratios, densities, and water contents based on the site's phase relationships and borehole conditions. Soil samples were made by combining light soil with 20% water and making three layers in split aluminum molds with fastening thermocouples at the mid-layer, as shown in Figure 4. To guarantee the repeatability and comparability of the test results, we carried out this procedure in the lab with great care.

Figure 4. Remolded soil samples with the same void ratio and degree of saturation

2.4. Test Equipment and Methods

The lack of commercially available equipment has discouraged research efforts in understanding artificial ground freezing on the shear strength properties of soils. This led to designing and manufacturing a device for triaxial shear frozen soil at the University of Technology-Iraq, as shown in Figure 5. The Laboratory tests will be conducted on the frozen soil at the Soil Mechanics Laboratory of the Civil Engineering Faculty.

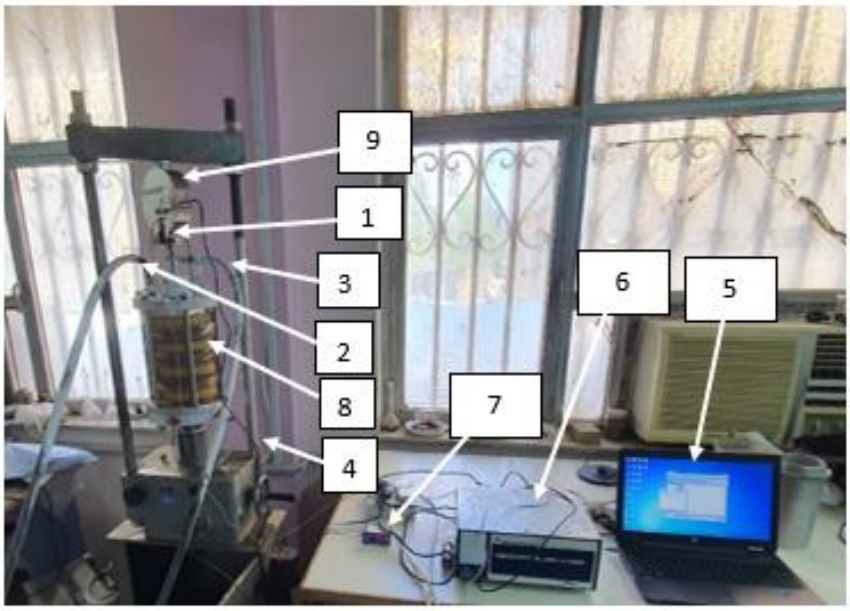

Figure 5. Apparatus for triaxial compression testing of frozen soil. 1. LVDT, 2. Cooling output 3. Cooling Input 4. Load Frame 5. Computing Device 6. Data Collection, 7. Thermocouple 8. Triaxial chamber; 9. load cell

3. Analysis of Uniaxial Compressive Strength Test Results

3.1. Shear Strength of Frozen Soil

Five temperature levels 0, -2, -5, -7, and -10 °C—were employed in the experimental uniaxial compressive strength tests to determine the mechanical properties of the frozen soil. Table 2 presents the test results, whereas Figure 6 illustrates the Mohr circle. The presence of ice crystals drastically alters the structure, strength, and other features of frozen soil compared to conventional soil. The compressive strength of frozen soil is directly influenced by variations in temperature. Unfrozen water transforms into ice crystals due to progressive alterations in the internal structure of frozen soil caused by a decrease in temperature. This alteration enhances the compressive strength of the soil.

Table 2. The results of the uniaxial compressive strength test

Temperature, °C	Deviatoric stress (Δσd), kN/ m²
0	164
-2	4300
-5	4700
-7	5800
-10	6210

3.2. Stress-Strain Curve Analysis

The experimental test result is illustrated in Figure 5. The frozen soil's stress-strain curves at various temperatures show deviatoric stress ($\Delta\sigma_d$) at five temperatures (0, -2, -5, -7, and -10 °C) under unconfining pressure (Figure 7-a). The coldest temperature (-10 °C) had the highest deviatoric stress, indicating a brittle failure with a clear break point and shear plane, as shown in Figure 7-b. The maximum deviatoric stress increased with temperature decrease from 0 to -10°C.

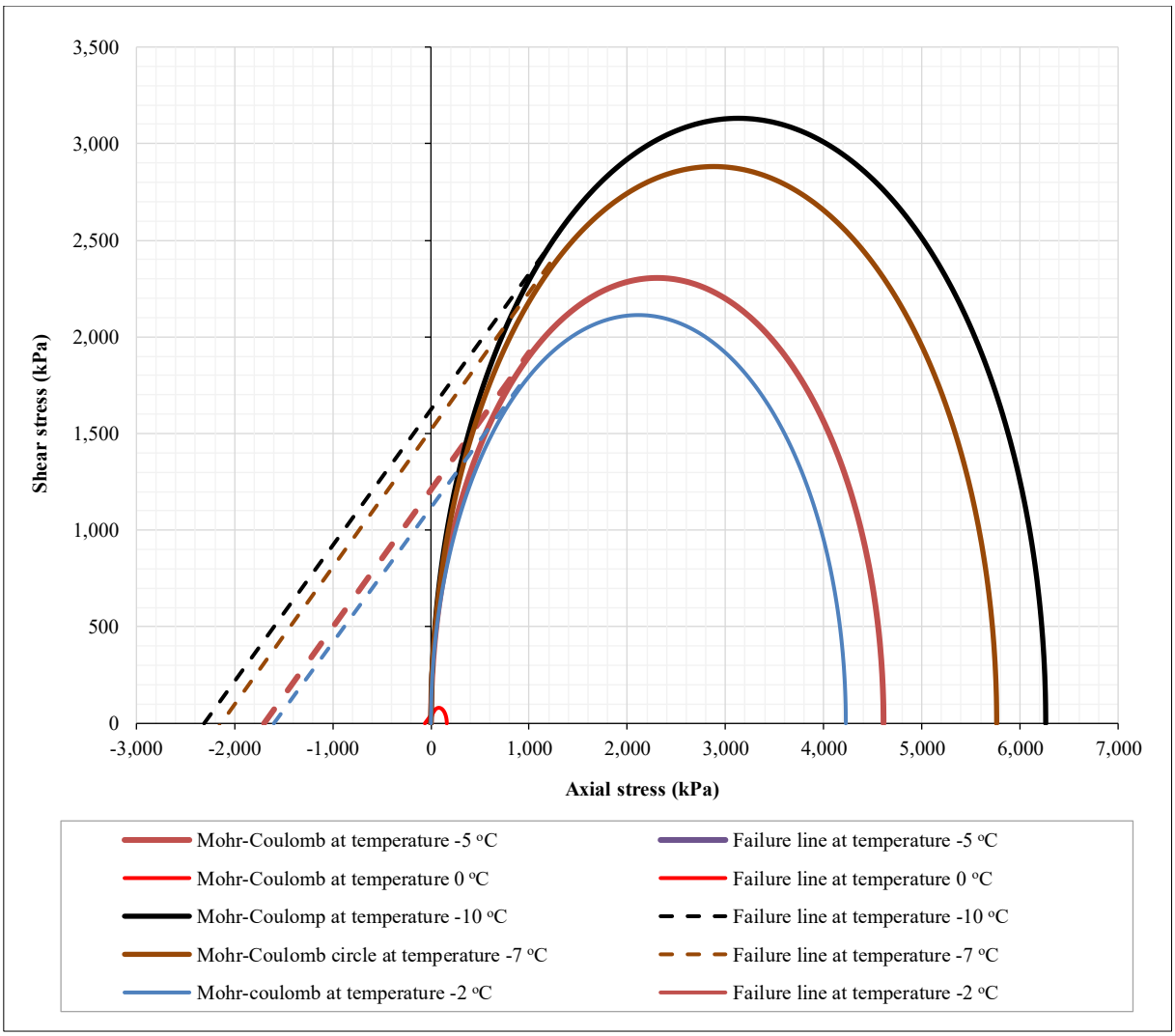

Figure 6. Mohr-Coulomb Circles of frozen sand at different temperatures

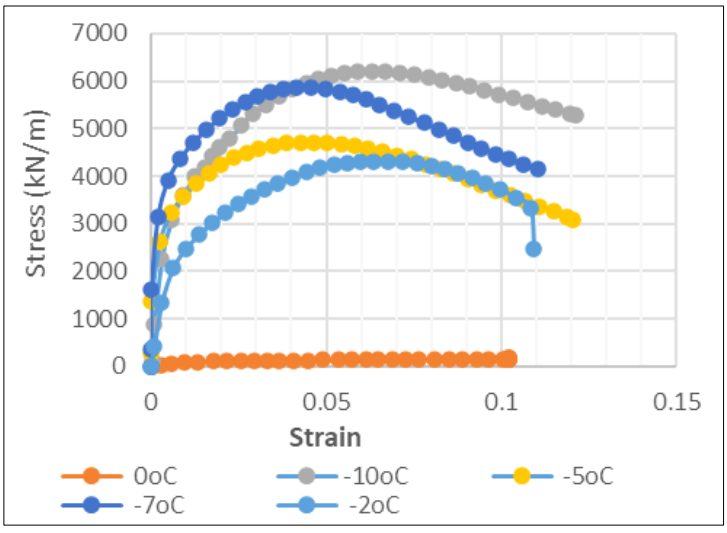

(a) Stress-strain curves of frozen sand at different temperatures

(b) Shear failure plane

Figure 7. Experimental test result

3.3. Analysis of the Impact of Temperature Decrease on the Tensile Stress of Frozen Soil

Figure 8 shows the nonlinear relationship between tensile stress and temperature drop, which aligns with other studies. The features of real frozen soil show that the connection between tensile strength and cooling suction is not a straight line [25, 26]. The tensile strength mechanism of warm frozen soil first arises from ice formation, followed by a

steady increase in the corresponding content. As the temperature decreases from 0 to -2°C, freezing transpires, rapidly reducing water content from the saturated to the residual conditions. Subsequently, the unfrozen water content persists, diminishing but at a reduced pace. This helps explain how quickly the soil's mechanical properties change in Figure 9 as the temperature decreases from 0 to -2 °C and falls from -2 to -10 °C. This aligns with the research conducted by Zhou et al. [27], which shows that ice constitutes around 85% of the overall tensile strength. In comparison, the enhancement of ice's tensile strength with a lower temperature contributes roughly 10% to the total strength. This is referred to as the "ice quality contribution." Tensile strength is mostly based on the chemical and physical bonds between the particle surfaces and the mix of ice and water, which makes up less than 5% of the whole. The ice content substantially affects the tensile strength of warm-frozen soil. Figure 9 depicts the tensile strength components of warm-frozen soil: (1) The quantity of ice enhances the overall tensile strength (I); (2) The strength of porous ice contributes to the total tensile strength (II); (3) The adhesion of soil particles to the ice and water augments the overall tensile strength (III).

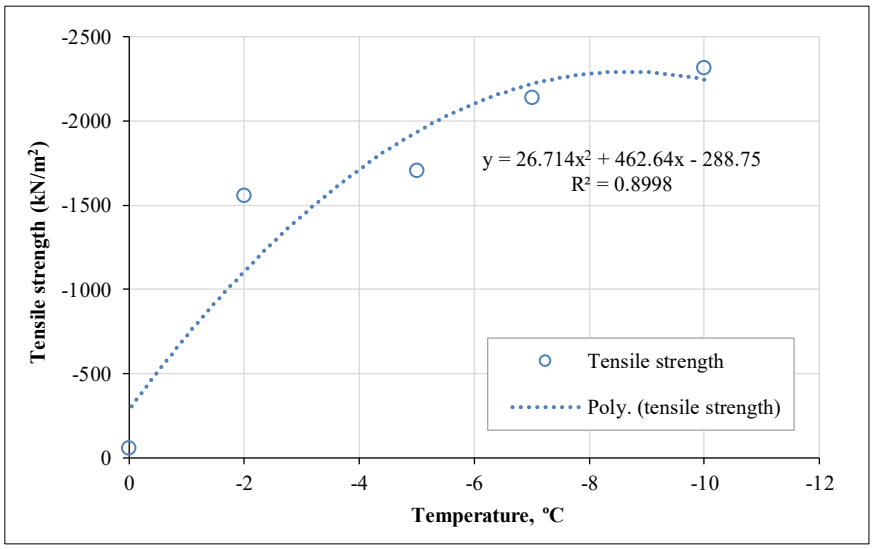

Figure 8. Relationship between total tensile strength for frozen soils and the tensile strength

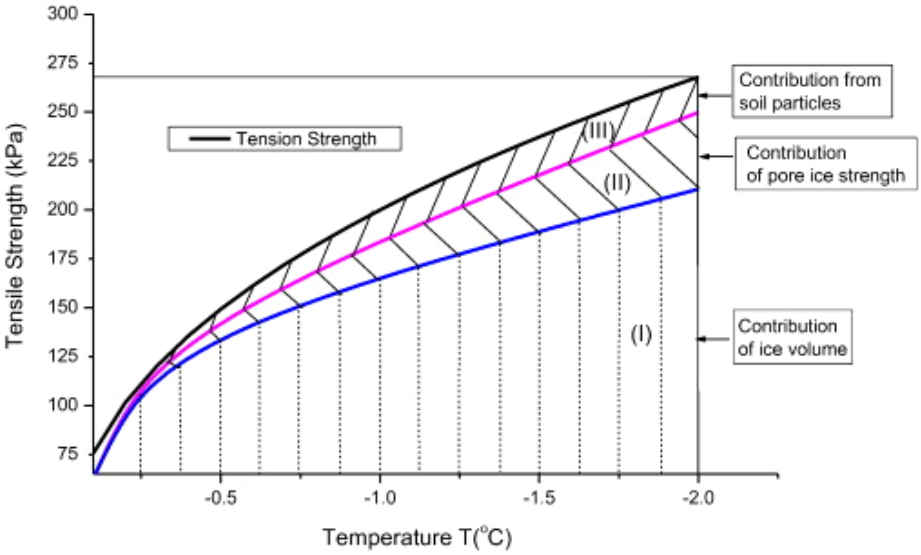

Figure 9. Tensile strength for warm frozen soils with temperature [27]

3.4. Evolution of Unconfined Compression Strength of Specimens with Soil Temperature Decrease

A linear function can depict the correlation between the temperature of frozen soil and its uniaxial compressive strength. The initial interval ranges from 0°C to -2°C, while the subsequent period extends from -2°C to -10°C. This indicates that the compressive strength of frozen soil escalates as the temperature decreases. It increases by 2068 kN/m² for each 1°C decrease from 0°C to -2°C and decreases to 238.75 kN/m² for each 1°C decrease from -2°C to -10°C. This is due to multiple variables. The presence of ice crystals in frozen soil alters its strength, structure, and other properties in comparison to unfrozen soil. Temperature variations have a direct impact on frozen soil's compressive strength. The internal composition of frozen soil progressively alters as the temperature decreases, causing unfrozen water to

crystallize into ice, hence enhancing the soil's compressive strength. Figure 10 illustrates the correlation between unconfined compressive strength and the temperature of frozen soil.

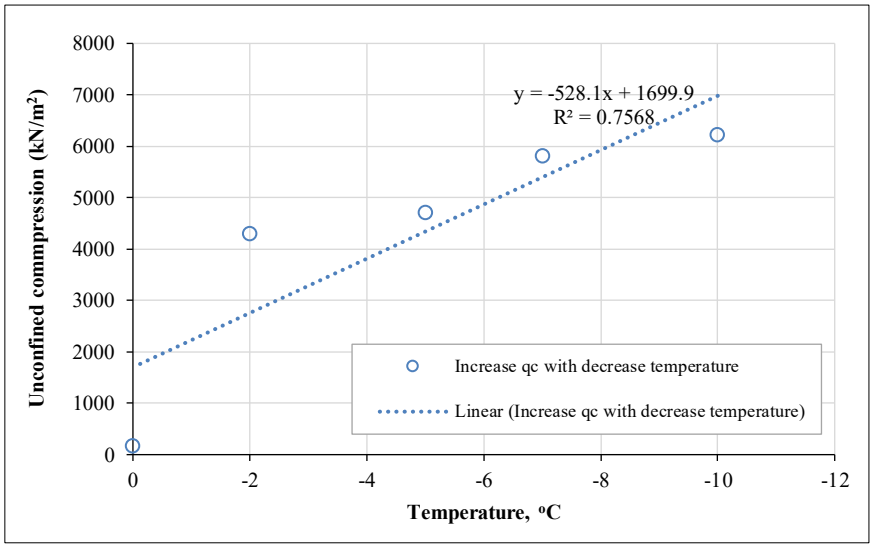

Figure 10. Relationship between unconfined compressive strength and temperature

3.5. Analysis of the Influence of Decreased Temperature on the Elastic Modulus of the Frozen Soil

Table 3 displays the frozen sand soil's elastic modulus as determined by testing. The relationship curves between temperature and elastic modulus for frozen soil samples are shown in Figure 11. The figure illustrates a linear relationship with a strong link between the elastic modulus of frozen soil and the freezing temperature across the examined temperature range. The elastic modulus increases by an average of 90,000 kN/m² for each degree the temperature decreases below 0°C. At any temperature within the testing temperature range, the interpolation approach can determine the matching soil layer's elastic modulus. The existence of ice crystals in frozen soil results from its distinct structure, strength, and other characteristics compared to regular soil. The change in temperature directly influences the compressive strength of frozen soil. As the temperature drops, the inside of frozen soil gradually changes. Unfrozen water turns into ice crystals, which connect the soil particles more strongly and increase its elastic modulus E.

Table 3. Elastic modulus testing results

Temperature, °C	Elastic Modulus, kN/m²
0	110000
-2	350000
-5	530000
-7	690000
-10	1000000

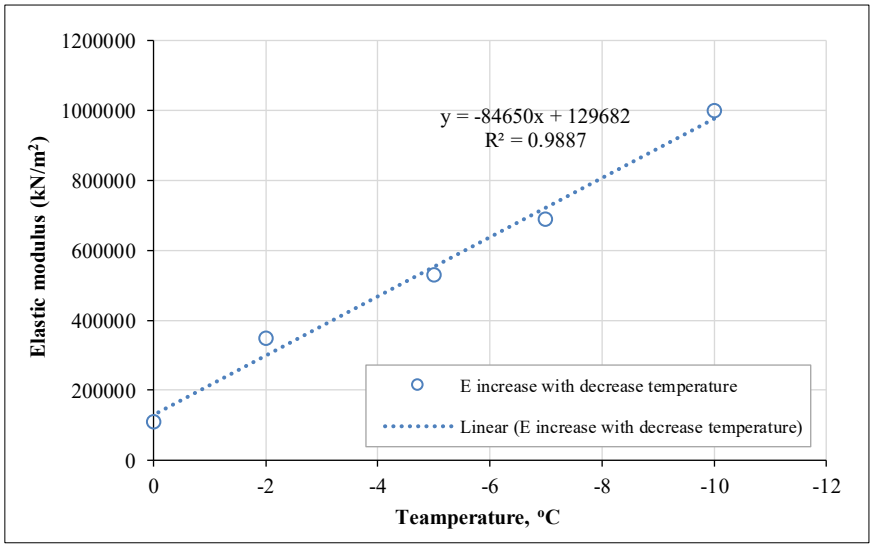

Figure 11. Correlation between elastic modulus and temperature

3.6. Analysis of the Impact of Decreased Temperature on the Apparent Cohesion of The Frozen Soil

When unfrozen soils, such as sand and gravel, are granular, the friction angle of the frozen soil will be similar to that of the unfrozen soil. This is supported by the Mohr's circle in Figure 12, which illustrates the Mohr-Coulomb failure envelopes of the frozen soil, so that according to Equation 1, the experimental test results in Table 2, and the Mohr's circle in Figure 6, the result in Table 4 and Figure 13 illustrates the apparent cohesiveness of the frozen soil. The findings within the tested temperature range show the apparent cohesiveness rises as the freezing temperature falls. This rise happens more quickly between 0°C and -2°C than between -2°C and -10°C. The rate of rise in apparent cohesiveness is 529 kN/m² for each 1-degree fall in temperature from 0°C to -2°C, while it decreases to 66.25 kN/m² for each 1-degree drop in temperature from -2°C to -10°C. The same rationale applies to the rise in uniaxial compressive strength.

$$\frac{\sigma_1-\sigma_3}{2} = (c\ cot\ \emptyset + \frac{\sigma_1-\sigma_3}{2})\ sin\emptyset \quad (1)$$

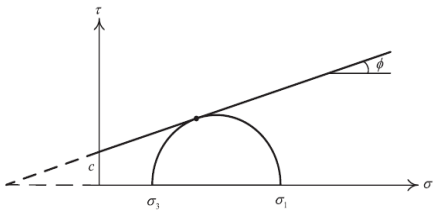

Figure 12. Illustrates the Mohr–Coulomb failure envelopes

Table 4. Test results of apparent cohesion with temperature

Temperature, °C	Apparent cohesion C (kN/m²)
0	42
-2	1100
-5	1200
-7	1500
-10	1630

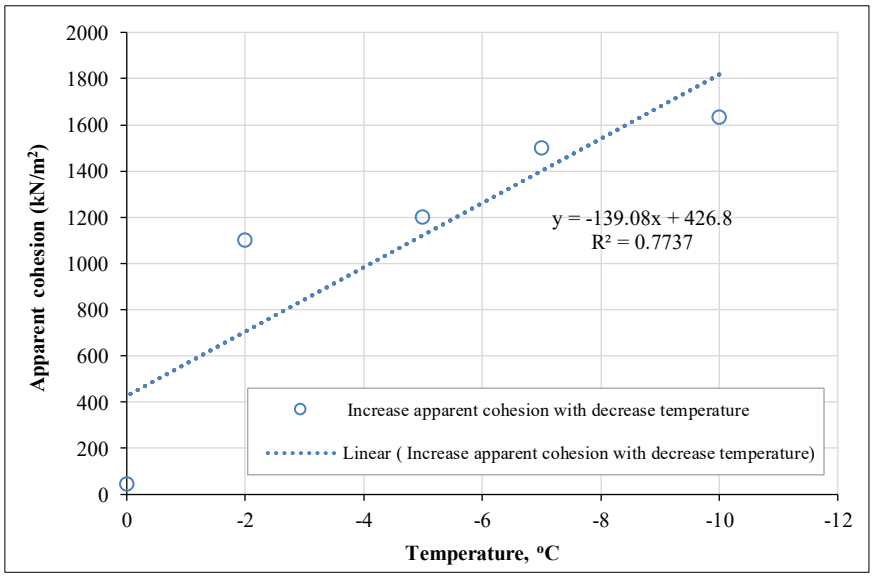

Figure 13. Relationship curve between apparent cohesion and temperature

4. Numerical Simulation Analysis

4.1. Numerical Model

The study used PLAXIS2D software to simulate confined pressure on samples that had different freezing temperatures. The Mohr-Coulomb and Hardening Soil models have been used to determine soil behavior. The model with dimensions of 1 m × 1 m, as shown in Figure 14. This corresponds to a quarter of the total soil sample size. This was done to take advantage of a symmetric axial geometry, and the weight of the soil was neglected in the program inputs in order to disregard the unrealistic model dimensions that were chosen to simplify the problem [28].

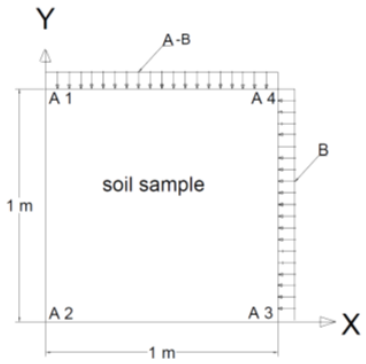

Figure 14. Illustrates the model size, applied load, and boundary conditions

The displacement parameters relative to the upper side (line A1-A4) and the right side (line A4-A3) are free to move, while the lower side (line A2-A3) and left sides (line A1-A2) are restricted to the direction perpendicular to the axis, while the free to move in the direction parallel to the axis due to symmetry. The left side (line A1-A2) and the bottom side (line A2-A3) of the geometry are the axes of symmetry. After setting the kind and magnitude of the applied loads in the input program, the calculation program was executed. By turning on or off the load in this instance's stage construction choice, the vertical load and the confined load were managed. The primary stresses σ'1 (load A) and σ'3 (load B) in the input are represented by distributed loads of 0, 300, 600, and 1200 kN/m², which are utilized to model the confinement pressure p', as illustrated in

The stage construction process in the calculation program allows for calculating all stages.

Phase 1: Initial Stage (k_o procedure)

Phase 2: Applied Confined pressure: we activate load B to apply the confinement pressure p' in this phase along the upper side (line A1-A4) and right side (line A4-A3).

Phase 3: Applied Deviatoric Stress

In this phase, the displacements are set to zero. The load applied by line displacement prescribed (displacement X = free, displacement Y = defined, distribution = uniform, Uy, start, ref = -0.25 m) along the upper boundary (line A1-A4) in the opposite directions of the axes while the horizontal load stays the same. Double-clicking the load in the geometry model will change Load A.

4.1.1. Mesh Sizes

Choosing the ideal mesh size is another factor to consider during finite element modeling. Very coarse mesh sizes might not be able to compute results and converge quickly enough, while very small mesh sizes might take too long. A sensitivity analysis was conducted on the first scenario to determine the optimal mesh size. Five distinct mesh sizes were considered in the mesh size sensitivity study: very coarse, coarse, medium, fine, and very fine. The stress-strain curve from different mesh size scenarios is compared in Figure 15. The stress-strain curve is influenced by mesh size, according to the results. It was found that the experimental stress-strain curve and the stress-strain curve with a fine mesh size were comparable. This demonstrated that the ideal mesh size was fine, which can produce precise results and quick computations. All of the models in this study were created using a fine mesh size.

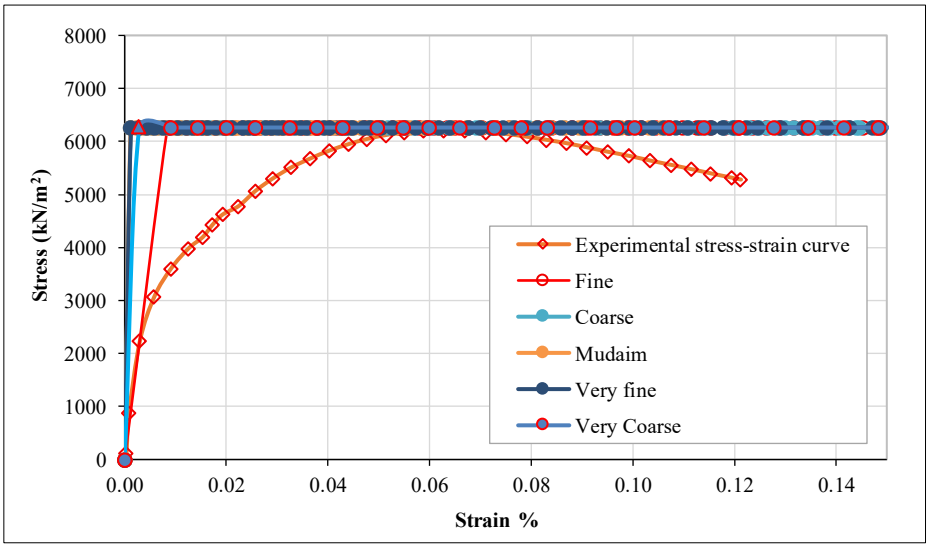

Figure 15. Stress-strain curve Comparison with Different Mesh Sizes

4.1.2. Parameter Calibration

The PLAXIS software calibrated the experimental parameters and soil properties derived from laboratory trials, which served as input data for the numerical simulation, as detailed in Table 5. Finite Element Method (FEM) was employed to create a numerical model of the triaxial compression test for frozen soil.

Table 5. Results of the uniaxial compressive strength tests of frozen soil.

Temperature, °C	Uniaxial compressive strength (kN/m²)	Apparent cohesion c (kN/m²)	E (kN/m²)	E50ref (kN/m²)
0	164	42	110000	10500
-2	4300	1100	350000	300000
-5	4700	1200	530000	780000
-7	5800	1500	690000	780000
-10	6210	1630	1000000	520000

4.1.3. Verification Numerical Model

This study utilized the uniaxial compressive strength test results of frozen soil from Table 5 as input data for numerical simulations in PLAXIS2D, aiming to compare the Mohr-Coulomb and Hardening Soil models with laboratory tests of sand through numerical stress-strain relationships. For every model, four scenarios were investigated with various setup parameters. The outcomes demonstrate that the test data and the computational results are consistent. The HS model's response transitions from elastic to plastic behavior, allowing a hyperbola to represent the correlation between axial strain and deviatoric stress (see Figures 16 to 20).

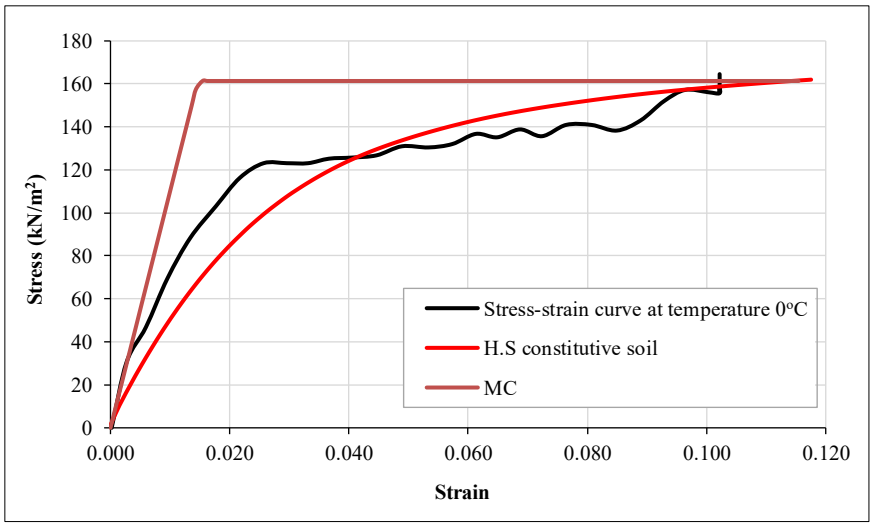

Figure 16. Experimental and numerical analysis of stress-strain curve at temperature 0 °C

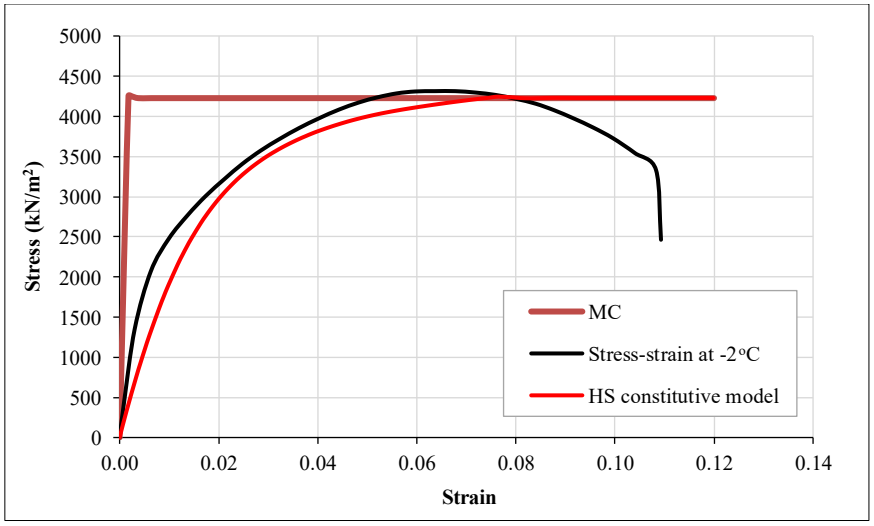

Figure 17. Experimental and numerical analysis of stress-strain curve at temperature -2 °C

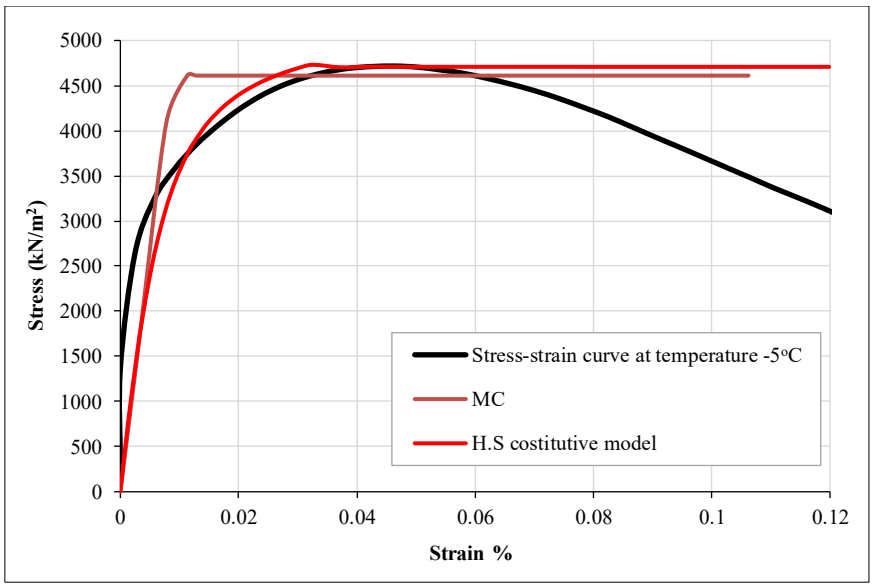

Figure 18. Experimental and numerical analysis of stress-strain curve at temperature -5 °C

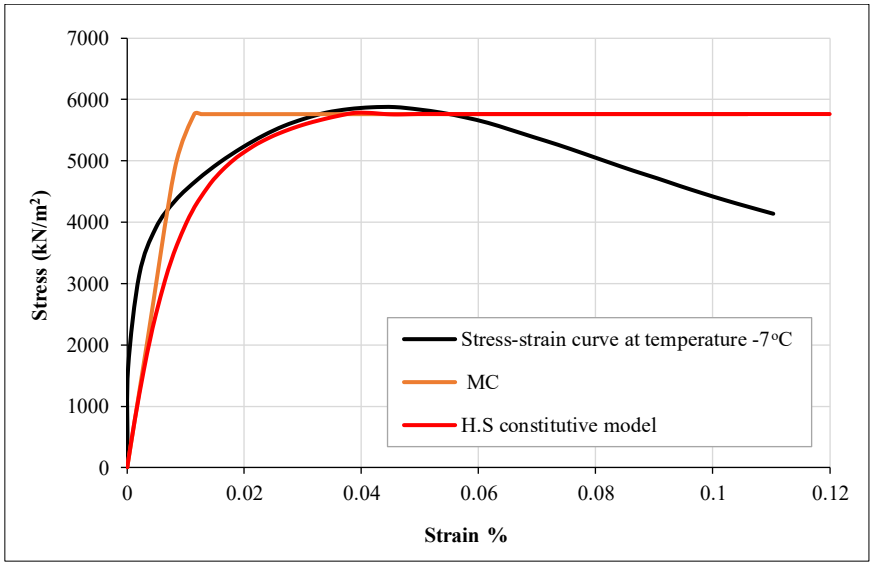

Figure 19. Experimental and numerical analysis of stress-strain curve at temperature -7 °C

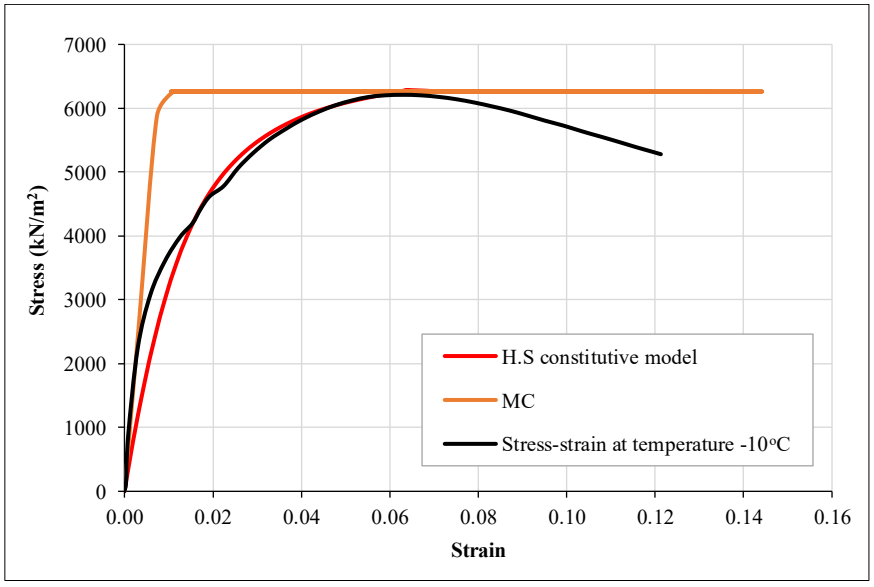

Figure 20. Experimental and numerical analysis of stress-strain curve at temperature -10 °C

4.2. Numerical Study Parameter at Decreased Temperature and Increased Confined Pressure

Evolution Stress-Strain Curve with Freezing Temperature Increase at Constant Confined Pressure

The numerical analysis results shown in Figure 21 are consistent with those reported in [29] Figure 22, indicating that under a fixed confining pressure, a reduction in temperature leads to a stiffer soil response. The stress–strain curve of frozen soil under these conditions exhibits three distinct stages.

- At first, the mixture has an elastic response with a nearly straight line, which means that there aren't many or any plastic stresses.
- At a certain threshold, plastic deformations begin.

In the end, softening will occur in regions where the stress-strain curves have negative slopes. The figure shows that a lower temperature results in a more rigid elastic response for both confining pressures. Moreover, lowering the temperature will render the soil mixture more brittle. Similar behavior was observed by Yamamoto & Springman [29].

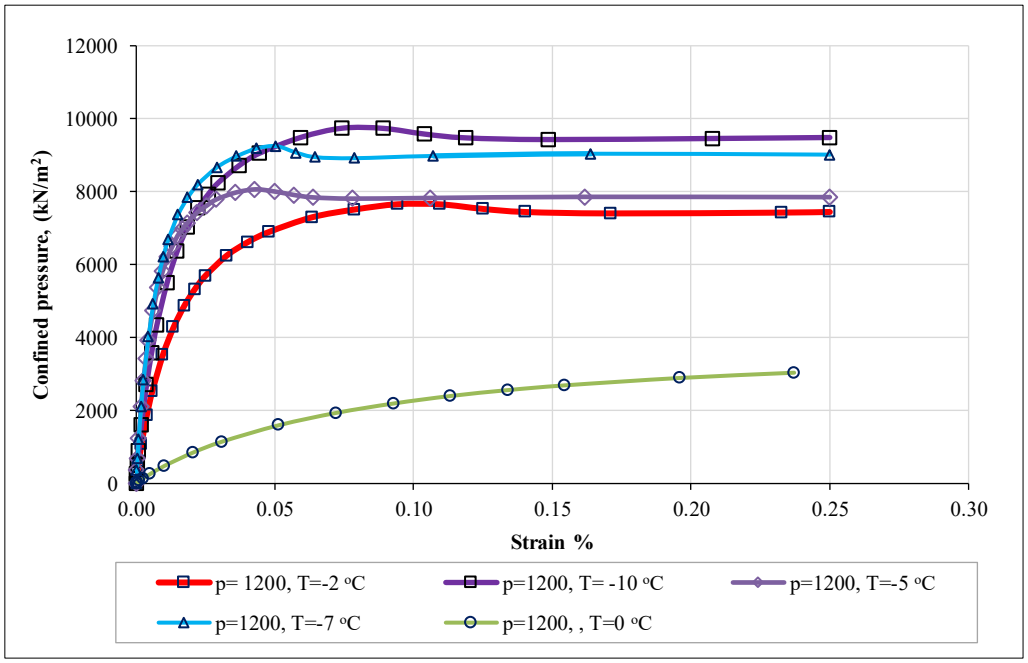

Figure 21. Stress-strain curve with varying temperature and constant confined pressure (1200 kN/m^2)

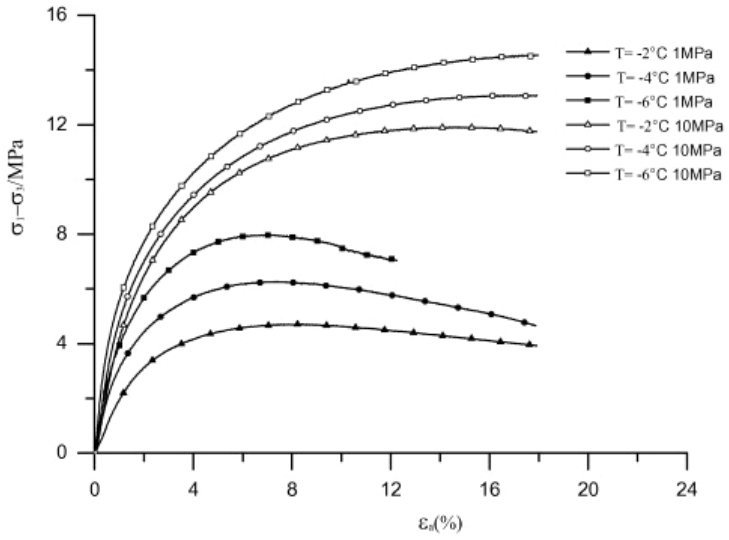

Figure 22. Show the stress-strain curves of frozen soil at two confining pressures over varying temperatures [29]

Evolution Stress-Strain Curve with Increased Confined Pressure at Constant Freezing

Several research studies, including those by Parameswaran & Jones [30] and Chamberlain et al. [31], have demonstrated the significant influence of confining pressure on the mechanical properties of frozen soils. At lower

confining pressures, frozen soils exhibit higher strength compared to unfrozen soils, and this strength increases as confining pressure rises. This effect is illustrated in Figure 22, where an increase in confining pressure at constant temperature results in a stiffer elastic response and higher peak shear stress. However, once the confining pressure exceeds a certain threshold, further increases reduce the maximum shear stress. Beyond this threshold, confining pressure initiates the pressure-induced melting of ice. As confining pressure continues to rise, more ice melts until the soil approaches a fully fluid-saturated state. When the ice content becomes insufficient for further melting, the soil transitions into a fully saturated condition, which leads to an increase in peak shear strength with additional increments in confining pressure.

Stress Path at Different Temperatures

Figures 23 to 27 represent the relationship between p-q with different confined pressures at the same temperature degree (0°C, -2°C, -5°C, -7°C, and -10°C). Also, the line of failure was drawn, which starts from the tensile stress value and meets with the stress path, which starts from p and rises by a rate equal to (1/3) q at the failure point. From Figures 23 to 27, it is noticed that in the case of constant temperature and increased confined pressure, there are several stress paths depending on the confined pressure, and all of these paths reach one failure line. The stress path increases by 1/3 of q. However, in the case of increased temperature and constant confined pressure, the opposite is true. There is one stress path, but several parallel failure lines point upwards. This means an increase in soil resistance, and at the same time, it means that the rate of effect of temperature is greater than confined pressure on increasing soil resistance, as shown in Figure 28.

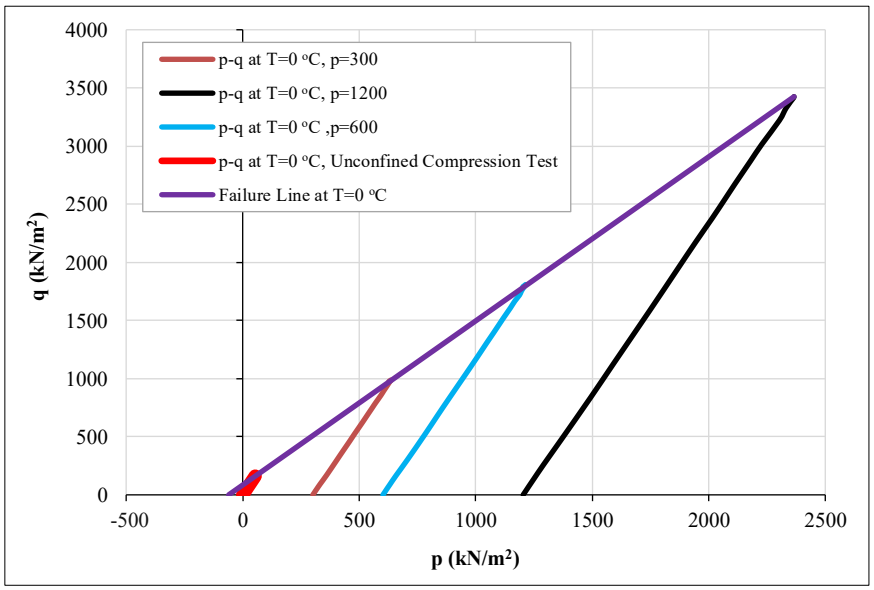

Figure 23. p-q diagram at temperature 0 °C with deferent confined pressure (0, 300, 600 and 1200 kN/m²)

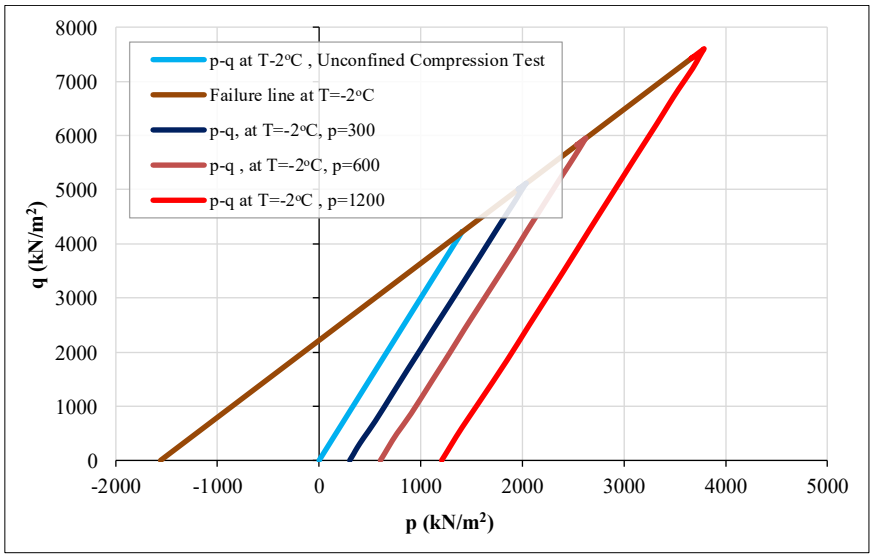

Figure 24. p-q diagram at temperature -2 °C with deferent confined pressure (0, 300, 600 and 1200 kN/m²)

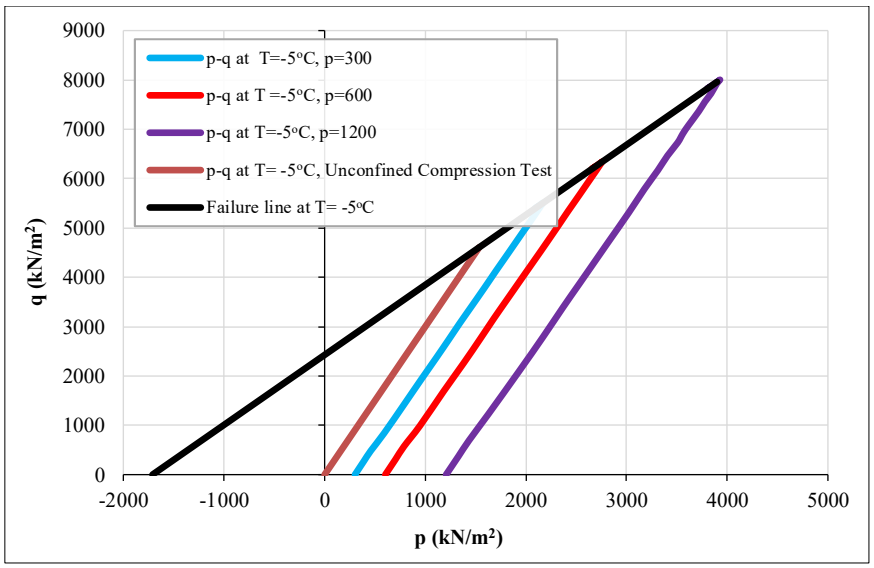

Figure 25. p-q diagram at temperature -5 °C with deferent confined pressure (0, 300, 600 and 1200 kN/m²)

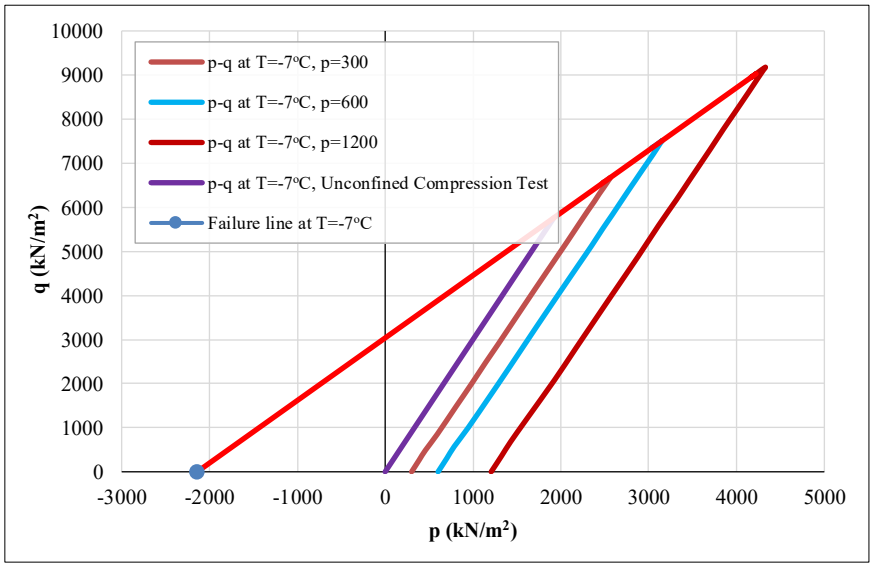

Figure 26. p-q diagram at temperature -7 °C with deferent confined pressure (0, 300, 600 and 1200 kN/m²)

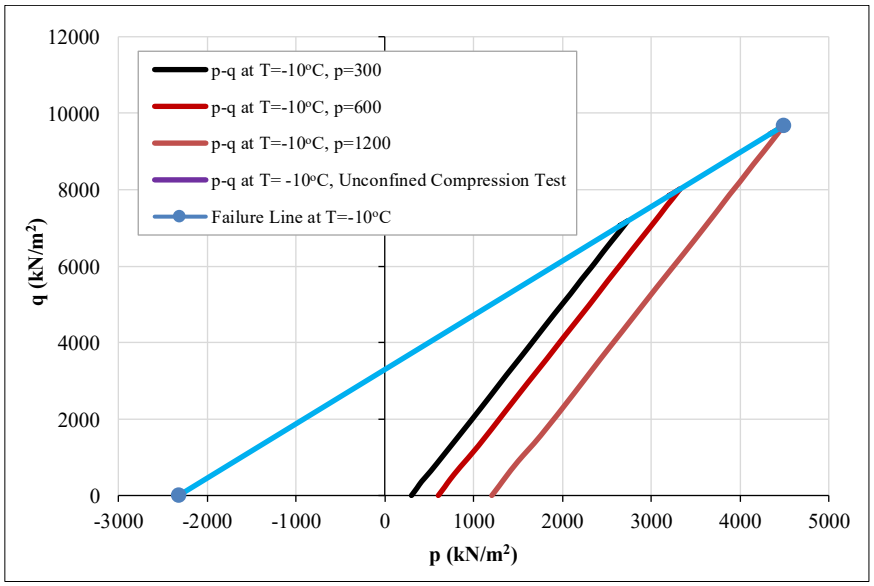

Figure 27. p-q diagram at temperature -10 °C with deferent confined pressure (300,600, 1200 kN/m²)

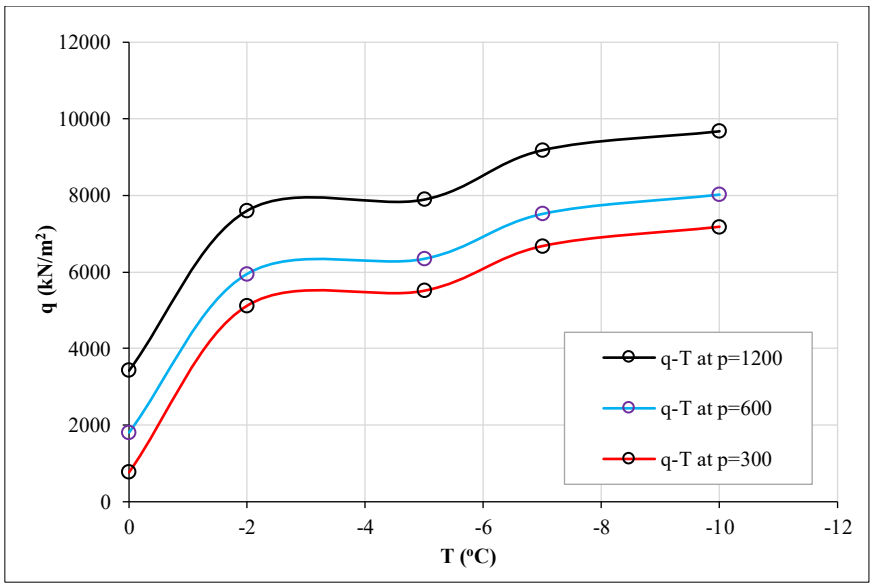

Figure 28. q-T relation with different confined pressures p (300, 600, 1200 kN/m²)

5. Conclusion

The experimental findings revealed a nearly linear increase in the elastic modulus, at a rate of about 90,000 kN/m² for each 1°C decrease below 0°C. The unconfined compressive strength exhibited a sharp increase of 2,068 kN/m² per degree from 0°C to −2°C, whereas within the range of −2°C to −10°C, the rate of increase was considerably lower at 529 kN/m² per degree. Similarly, apparent cohesion rose by 238.75 kN/m² per degree in the range of 0°C to −2°C, while from −2°C to −10°C, the rate of increase reduced to 66.25 kN/m² per degree. The numerical stress–strain curves closely matched the experimental observations, displaying strain-hardening behavior under normal conditions but transitioning to strain-softening under freezing conditions. Additionally, the results highlighted a nonlinear relationship between temperature reduction and tensile stress increase, underscoring the complex mechanical response of soils under sub-zero conditions.

6. Declarations

6.1. Author Contributions

Conceptualization, W.R.H. and H.H.K.; methodology, W.R.H.; software, W.R.H.; validation, W.R.H., H.H.K., and S.F.A.; formal analysis, H.H.K.; investigation, S.F.A.; resources, W.R.H.; data curation, S.F.A.; writing—original draft preparation, S.F.A.; writing—review and editing, H.H.K.; visualization, W.R.H.; supervision, H.H.K.; project administration, W.R.H.; funding acquisition, H.H.K. All authors have read and agreed to the published version of the manuscript.

6.2. Data Availability Statement

The data presented in this study are available in the article.

6.3. Funding

The authors received no financial support for the research, authorship, and/or publication of this article.

6.4. Conflicts of Interest

The authors declare no conflict of interest.

7. References

[1] Bragg, R. A., & Andersland, O. B. (1981). Strain rate, temperature, and sample size effects on compression and tensile properties of frozen sand. Engineering Geology, 18(1–4), 35–46. doi:10.1016/0013-7952(81)90044-2.

[2] Xu, X., Lai, Y., Dong, Y., & Qi, J. (2011). Laboratory investigation on strength and deformation characteristics of ice-saturated frozen sandy soil. Cold Regions Science and Technology, 69(1), 98–104. doi:10.1016/j.coldregions.2011.07.005.

[3] Liu, J., Lv, P., Cui, Y., & Liu, J. (2014). Experimental study on direct shear behavior of frozen soil–concrete interface. Cold Regions Science and Technology, 104–105, 1–6. doi:10.1016/j.coldregions.2014.04.007.

[4] Li, K. Q., Yin, Z. Y., Jin, Y. F., & Liu, Y. (2025). Investigation on evolution law of frozen wall thickness in artificial ground freezing under seepage conditions. Canadian Geotechnical Journal, 62, 1–21. doi:10.1139/cgj-2023-0576.

[5] Li, K. Q., Yin, Z. Y., Qi, J. L., & Liu, Y. (2024). State-of-the-Art Constitutive Modelling of Frozen Soils. Archives of Computational Methods in Engineering, 31(7), 3801–3842. doi:10.1007/s11831-024-10102-w.

[6] Hu, X. D., & Chen, R. (2006). Construction technology of freezing method applied to cross-passage of double-deck cross-river road tunnel. Low Temperature Architecture Technology, 5, 64–66.

[7] Cai, C., Ma, W., Zhou, Z., Mu, Y., Zhao, S., Chen, D., & Liao, M. (2019). Laboratory investigation on strengthening behavior of frozen China standard sand. Acta Geotechnica, 14(1), 179–192. doi:10.1007/s11440-018-0648-3.

[8] Fish, A. M., & Zaretsky, Y. K. (1997). Ice Strength as a Function of Hydrostatic Pressure and Temperature. Defense Technical Information Center, CRREL976. doi:10.21236/ada333030.

[9] Li, K. Q., Li, D. Q., & Liu, Y. (2020). Meso-scale investigations on the effective thermal conductivity of multi-phase materials using the finite element method. International Journal of Heat and Mass Transfer, 151, 119383. doi:10.1016/j.ijheatmasstransfer.2020.119383.

[10] Yang, Z. J., Still, B., & Ge, X. (2015). Mechanical properties of seasonally frozen and permafrost soils at high strain rate. Cold Regions Science and Technology, 113, 12–19. doi:10.1016/j.coldregions.2015.02.008.

[11] Lai, Y., Jin, L., & Chang, X. (2009). Yield criterion and elasto-plastic damage constitutive model for frozen sandy soil. International Journal of Plasticity, 25(6), 1177–1205. doi:10.1016/j.ijplas.2008.06.010.

[12] He, J., Niu, F., Su, W., & Jiang, H. (2023). Nonlinear unified strength criterion for frozen soil based on homogenization theory. Mechanics of Advanced Materials and Structures, 30(19), 4002–4015. doi:10.1080/15376494.2022.2087126.

[13] Lai, Y., Xu, X., Dong, Y., & Li, S. (2013). Present situation and prospect of mechanical research on frozen soils in China. Cold Regions Science and Technology, 87, 6–18. doi:10.1016/j.coldregions.2012.12.001.

[14] Li, K. Q., Yin, Z. Y., & Liu, Y. (2023). Influences of spatial variability of hydrothermal properties on the freezing process in artificial ground freezing technique. Computers and Geotechnics, 159, 105448. doi:10.1016/j.compgeo.2023.105448.

[15] Liu, Y., Li, K. Q., Li, D. Q., Tang, X. S., & Gu, S. X. (2022). Coupled thermal–hydraulic modeling of artificial ground freezing with uncertainties in pipe inclination and thermal conductivity. Acta Geotechnica, 17(1), 257–274. doi:10.1007/s11440-021-01221-w.

[16] Zhou, J., Zhao, W., & Tang, Y. (2022). Practical prediction method on thaw deformation of soft clay subject to artificial ground freezing based on elaborate centrifuge modeling experiments. Tunnelling and Underground Space Technology, 122, 104352. doi:10.1016/j.tust.2021.104352.

[17] Li, K. Q., Yin, Z. Y., Zhang, N., & Liu, H. C. (2025). Physics-informed neural networks for solving steady-state temperature field in artificial ground freezing. Canadian Geotechnical Journal, 62, 1–17. doi:10.1139/cgj-2024-0650.

[18] French, H. (2003). The development of periglacial geomorphology: 1- up to 1965. Permafrost and Periglacial Processes, 14(1), 29–60. doi:10.1002/ppp.438.

[19] Yu, X., Zheng, G., Zhou, H., & Ma, F. (2025). Analytical solutions for the stability of stone column-supported and geosynthetic-reinforced embankment. Canadian Geotechnical Journal, 62, 1–15. doi:10.1139/cgj-2023-0314.

[20] Xu, K., Zhang, N., Yin, Z. Y., & Li, K. (2025). Finite element-integrated neural network for inverse analysis of elastic and elastoplastic boundary value problems. Computer Methods in Applied Mechanics and Engineering, 436, 117695. doi:10.1016/j.cma.2024.117695.

[21] Zhang, N., Xu, K., Yu Yin, Z., Li, K. Q., & Jin, Y. F. (2025). Finite element-integrated neural network framework for elastic and elastoplastic solids. Computer Methods in Applied Mechanics and Engineering, 433, 117474. doi:10.1016/j.cma.2024.117474.

[22] Yuanming, L., Yugui, Y., Xiaoxiao, C., & Shuangyang, L. (2010). Strength criterion and Elastoplastic constitutive model of frozen silt in generalized plastic mechanics. International Journal of Plasticity, 26(10), 1461–1484. doi:10.1016/j.ijplas.2010.01.007.

[23] Zhu, Y., & Carbee, D. L. (1984). Uniaxial compressive strength of frozen silt under constant deformation rates. Cold Regions Science and Technology, 9(1), 3–15. doi:10.1016/0165-232x(84)90043-0.

[24] Mayoralty of Baghdad. (2025). Mayoralty of Baghdad, Baghdad, Iraq. Available online: https://amanatbaghdad.gov.iq/en (accessed on July 2025).

[25] Azmatch, T. F., Sego, D. C., Arenson, L. U., & Biggar, K. W. (2011). Tensile strength and stress-strain behaviour of Devon silt under frozen fringe conditions. Cold Regions Science and Technology, 68(1–2), 85–90. doi:10.1016/j.coldregions.2011.05.002.

[26] Akagawa, S., & Nishisato, K. (2009). Tensile strength of frozen soil in the temperature range of the frozen fringe. Cold Regions Science and Technology, 57(1), 13–22. doi:10.1016/j.coldregions.2009.01.00.

[27] Zhou, G., Hu, K., Zhao, X., Wang, J., Liang, H., & Lu, G. (2015). Laboratory investigation on tensile strength characteristics of warm frozen soils. Cold Regions Science and Technology, 113, 81–90. doi:10.1016/j.coldregions.2015.02.003.

[28] PLAXIS 2D. (2021). Material Models Manual 2D. Bentley Communities: Exton, United States.

[29] Yamamoto, Y., & Springman, S. M. (2014). Axial compression stress path tests on artificial frozen soil samples in a triaxial device at temperatures just below 0 °C. Canadian Geotechnical Journal, 51(10), 1178–1195. doi:10.1139/cgj-2013-0257.

[30] Parameswaran, V. R., & Jones, S. J. (1981). Triaxial testing of frozen sand. Journal of Glaciology, 27(95), 147–155. doi:10.1017/S0022143000011308.

[31] Chamberlain, E., Groves, C., & Perham, R. (1972). The mechanical behaviour of frozen earth materials under high pressure triaxial test conditions. Géotechnique, 22(3), 469–483. doi:10.1680/geot.1972.22.3.469.